

## Epitaxial growth and optical transitions of cubic GaN films

D. Schikora, M. Hankeln, D. J. As, and K. Lischka

Universität Paderborn, FB 6-Physik, Warburgerstraße 100, D-33098 Paderborn, Germany

T. Litz and A. Waag

Universität Würzburg, Physikalisches Institut, Am Hubland, D-97074 Würzburg, Germany

T. Buhrow and F. Henneberger

Humboldt-Universität Berlin, Institut für Physik, Invalidenstraße 110, D-10115 Berlin, Germany

(Received 6 May 1996)

Single-phase cubic GaN layers are grown by plasma-assisted molecular-beam epitaxy. The temperature dependence of the surface reconstruction is elaborated. The structural stability of the cubic growth in dependence of the growth stoichiometry is studied by RHEED measurements and numerical simulations of the experimental RHEED patterns. Growth oscillations on cubic GaN are recorded at higher substrate temperatures and nearly stoichiometric adatom coverage. Photoluminescence reveals the dominant optical transitions of cubic GaN and, by applying an external magnetic field, their characteristic  $g$  factors are determined. [S0163-1829(96)51936-3]

Recently, it has been demonstrated that blue light-emitting diodes and even laser diodes can be fabricated from GaN-based heterostructures grown on sapphire(0001) substrates.<sup>1,2</sup> The polytype group-III nitrides are naturally stable in the hexagonal wurtzite structure ( $h$ -III-N). Nevertheless, successful epitaxial growth of the metastable cubic phase of GaN ( $c$ -GaN) has been accomplished by various groups in the past.<sup>3,4</sup> In comparison with  $h$ -GaN, the cubic modification offers several technological advantages, in particular, easy cleavage. The major difficulty in the growth of  $c$ -GaN originates from the polytypism and, as a result, an increased tendency of forming wurtzite-phase subdomains within the cubic lattice. The phase purity of molecular-beam-epitaxy (MBE) grown  $c$ -GaN on GaAs substrates has been the subject of several previous studies,<sup>5-7</sup> emphasizing the crucial role of the surface stoichiometry. In this paper, the temperature dependence of the surface reconstruction on the atomic N/Ga flux ratio as well as the structural mechanism of the zinc-blende-wurtzite transition are studied by reflection high-energy electron diffraction (RHEED). Unlike Ref. 8, where  $c$ -GaN crystallites grown in a liquid-phase-like process were investigated, we aim at the fabrication of highly homogeneous cubic epilayers. The dominant optical transitions in these films are elucidated by photoluminescence (PL) measurements, including the magnetic field behavior.

The single-phase  $c$ -GaN layers were grown on GaAs(001) substrates by plasma-assisted MBE using a Riber-32 system equipped with elemental sources of Ga and As and an Oxford Applied Research CARS 25 rf activated plasma source. The  $N_2$ -background pressure in the growth chamber was varied between  $2 \times 10^{-4}$  and  $5 \times 10^{-3}$  Pa. Before starting the  $c$ -GaN nucleation, a GaAs buffer layer was grown first at 600 °C under  $(2 \times 4)$  reconstruction to ensure As-stabilized conditions. The nucleation of  $c$ -GaN was initiated at the same substrate temperature using a N/Ga flux ratio of about 4. After deposition of 10–20 ML, the nucleation stage was stopped and the substrate temperature subsequently raised to

680–740 °C. The static GaN(001) surface exhibits a clear  $(2 \times 2)$  reconstruction during this period. The growth was continued at this higher temperature level varying the N/Ga flux ratio and the substrate temperature. The growth process was monitored continuously by RHEED and RHEED image recording systems.

The reconstruction of the growing surface is controlled mainly by surface stoichiometry. Work on III-V (GaAs) as well as II-VI (ZnSe) compounds has proven the coincidence between reconstruction boundaries and isoatom coverage contours.<sup>9,10</sup> Figure 1 depicts the surface reconstruction diagram of  $c$ -GaN measured during growth. The V/III flux ratio is plotted versus growth temperature. In this ratio, the Ga flux rate is related to the flux rate of atomic N. We have

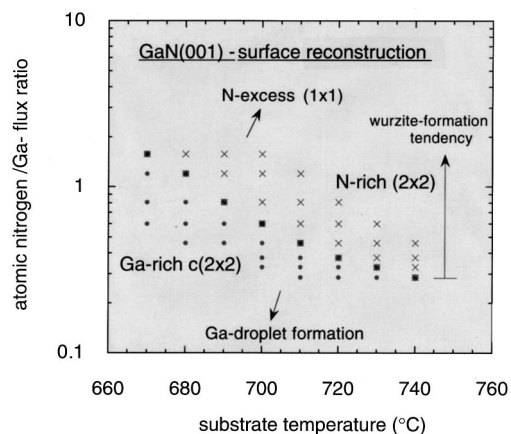


FIG. 1. Surface reconstruction of zinc-blende GaN(001) in dependence of the growth temperature and the N/Ga flux ratio. The dots represent the stability range of the Ga-rich  $c(2 \times 2)$  reconstruction, the crosses show the stability range of the N-rich  $(2 \times 2)$  reconstruction. A superposition of both reconstructions occurs in a narrow range in between, indicating near stoichiometric compositions.

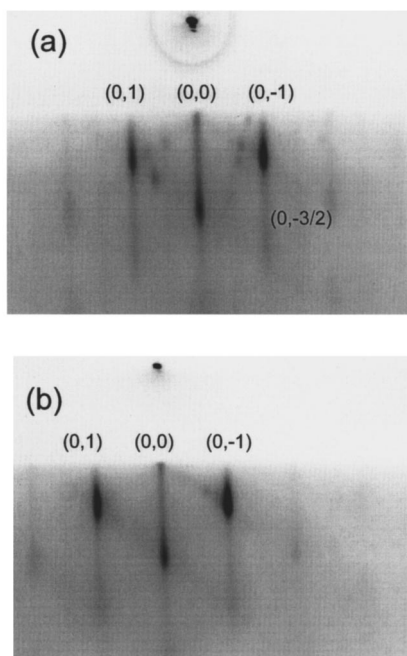


FIG. 2. GaN(001) RHEED patterns along the  $[110]$  azimuth for two different N/Ga ratios. The pattern in (a) represents N-rich conditions with a N/Ga ratio of about 0.5; the pattern in (b) demonstrates near stoichiometric, Ga-rich conditions with a N/Ga ratio of 0.35 at a growth temperature of about  $720^\circ\text{C}$ .

found by mass-spectrometric measurements that the effective flow of atomic N arriving on the surface amounts to 1–7 % of the  $\text{N}_2$ -beam-equivalent pressure, mainly depending on the total flow rate and the rf power applied. In addition to the static  $(2 \times 2)$  reconstruction, we have observed  $c(2 \times 2)$  and  $(2 \times 2)$  reconstructions as well as an unreconstructed  $(1 \times 1)$  surface during the growth, in accordance with previously published results.<sup>7</sup> At high excess of N, the unreconstructed  $(1 \times 1)$  surface is stable. Under Ga-stabilized conditions, a  $c(2 \times 2)$  reconstruction appears; layers grown here show  $n$ -type conductivity in Hall-effect measurements. The  $(2 \times 2)$  reconstruction is associated with N-stabilized conditions giving rise to  $p$ -type behavior. In a narrow range between the  $c(2 \times 2)$  and  $(2 \times 2)$  regime, both reconstructions occur simultaneously with different intensities of the reconstruction lines, indicating a nearly stoichiometric adatom coverage. At temperatures lower than  $680^\circ\text{C}$ , this requires a N/Ga flux ratio of about 1. For substrate temperatures greater than  $700^\circ\text{C}$ , the Ga reevaporation becomes significant. The Ga loss from the surface must be compensated to stabilize stoichiometric conditions. Therefore, the N/Ga ratio decreases. Assuming that the Ga desorption is the dominant kinetic process limiting the growth rate, we have calculated the respective activation energy. From the slope of the stoichiometric line, we find  $E_{\text{des}}^{\text{Ga}} = 2.11 \text{ eV} \pm 0.2 \text{ eV}$  by an Arrhenius plot. This is much lower than the value of 3.2 eV estimated from Gas-Source MBE data.<sup>11</sup>

The role of surface stoichiometry is illustrated in Fig. 2, the patterns in Figs. 2(a) and 2(b) are contrast inverted for better visibility. Both RHEED patterns were taken along the  $[110]$  azimuth of GaN(001) during the growth. The flux ratio in (a) was set at 0.5 to guarantee a slight excess of N for the

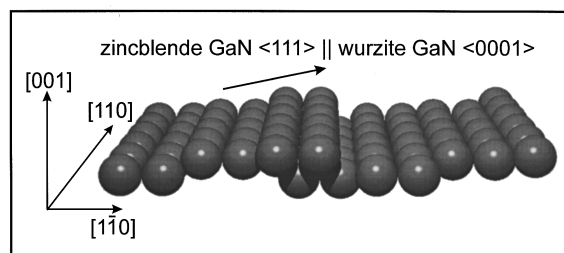


FIG. 3. Model of the zinc-blende–wurtzite phase transition of GaN based on numerical calculations of the RHEED pattern. Assuming a parallel orientation of the hexagonal  $c$  axis with respect to the cubic  $\langle 111 \rangle$  direction, the growing (001)GaN surface forms a ‘‘roof-tile’’-like surface profile. The corresponding surface structure, which yields the experimental RHEED reflex pattern of Fig. 2(a), is illustrated. Only the positions of the Ga atoms are sketched.

growth temperature of about  $720^\circ\text{C}$ . The integral order beams of  $c$ -GaN and the reconstruction line at  $(0, -3/2)$  are clearly visible. Besides this, additional reflexes appear in the pattern which are obviously associated with another structural phase and also with a formation of growth facets. The pattern in 2(b) demonstrates that the occurrence of these extra reflexes can be influenced by changing the growth stoichiometry, e.g., reducing the N excess. The flux ratio was decreased from 0.50 to 0.35 in this particular case. Both patterns were recorded during the same growth experiment. The additional reflexes are almost absent in pattern 2(b); photograph 2(b) was taken 60 min after the flux-parameter correction.

To understand the structural origin of these extra reflexes in the RHEED images, we have performed numerical calculations of the RHEED pattern within a kinematical model. Different atom arrangements of the (001) surface were assumed in our simulations to reproduce their reflex positions. We have found that these extra reflexes can be attributed to a wurtzite phase with  $c$  axis oriented parallel to the  $\langle 111 \rangle$  axis of the zinc-blende structure. The beginning of the transformation from the cubic into the wurtzite structure is manifested by a superposition of both the integral order reflexes of the cubic phase and the additional reflexes of the wurtzite phase in the experimental RHEED pattern [see Fig. 2(a)]. Figure 3 presents a schematics of the surface structure yielding the experimental RHEED pattern of Fig. 2(a). For simplicity, only the Ga atoms are sketched. The picture represent the modified positions of Ga atoms forming a ‘‘roof-tile’’-like surface profile with increased roughness on the growing surface during the initial stage of the phase transformation process.

Under optimum flux-ratio conditions of about 0.30 and at substrate temperatures of  $740^\circ\text{C}$ , we have succeeded in detecting RHEED oscillations at the specular spot position in the  $[\bar{1}10]$  azimuth. At these growth conditions the tendency to form mixed phases is suppressed and the growth becomes increasingly two-dimensional due to the enhanced surface mobility of the Ga adatoms. The oscillations shown in Fig. 4 appear after growth interruption and opening of the Ga-cell shutter. The steep initial rise of the specular spot intensity suggests that the growth onset is accompanied by an effec-

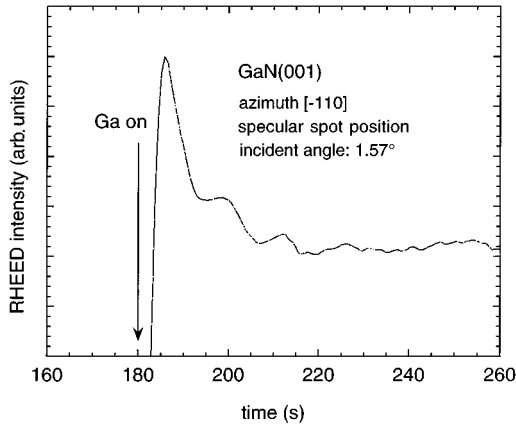


FIG. 4. RHEED oscillations of *c*-GaN(001) detected at the specular spot position in the  $[\bar{1}10]$  azimuth. The angle of incidence of about  $1.57^\circ$  indicates an out-of-phase condition.

tive surface smoothing. The oscillations are rapidly damped and entirely disappear when the specular beam intensity is recovered to its steady-state level. A growth rate of about 0.08 ML/sec is deduced from the oscillation period. This value is in remarkable agreement with the growth rate derived from the total layer thickness measured by optical interference spectroscopy (FTIR).

For the PL measurements, the samples were mounted in the bore of a split-coil magnetocryostat capable of fields up to  $B=12$  T. The 351-nm line of an Argon-ion laser was used for above-gap excitation. The magnetic field was perpendicular to the GaN layer plane (Faraday geometry), the excitation intensity was in the  $100 \text{ W/cm}^2$  range, and the bath temperature was 1.6 K. The PL was detected in a backward geometry and decomposed by a  $\lambda/4$  plate into circular polarizations  $\sigma^+$  and  $\sigma^-$ , respectively. At zero  $B$  field, the PL spectrum (see Fig. 5) exhibits three pronounced lines above 3.05 eV and two weaker structures on the low-energy side. Those features are present in all samples; their intensity ratio is, however, sensitive to the growth conditions. Since the width of the PL bands ( $>10$  meV) is considerably larger than the typical magnetic energies ( $<1$  meV), a direct observation of the field-induced Zeeman splittings was not possible. However, these splittings are manifested by an increasing degree of  $\sigma^-$  polarization ( $P$ ) being characteristic for the initial state of the respective emission process. Assuming an energy separation  $\Delta E = g\mu_B B$  between the two splitoff components giving rise to  $\sigma_{\pm}$  emission, it holds that

$$P = \frac{I^- - I^+}{I^- + I^+} = \tanh\left(\frac{\Delta E}{2k_B T}\right)$$

with  $g$  representing an effective  $g$  factor and  $T$  the carrier temperature. In order to extract  $P$  as a function of  $B$  for the various transitions, we have carefully decomposed the PL spectrum into a sum of Gaussian bands. The inset of Fig. 5 displays the result for the three dominant PL peaks. For the evaluation of the  $g$  factors, we have used  $T=1.6$  K in the

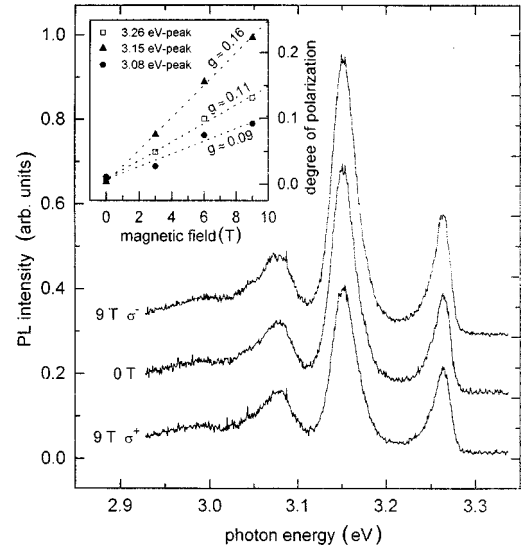


FIG. 5. Low-temperature (1.6 K) photoluminescence spectra of a *c*-GaN film of  $1.2\text{-}\mu\text{m}$  layer thickness in zero magnetic field and at a field of 9 T in Faraday configuration decomposed in  $\sigma^+$  and  $\sigma^-$  polarization under above-bandgap excitation (351 nm,  $100 \text{ W/cm}^2$ ). The inset shows the dependence of the degree of polarization on the magnetic field for the dominating features at 3.26, 3.15, and 3.08 eV and their effective  $g$  factors.

above formula. Since the actual carrier temperature might be somewhat larger, these values represent, in a strict sense, lower limits.

The energy of the free exciton (FX) and the band gap of *c*-GaN is still under debate.<sup>12–15</sup> From the fact that no further transition is observable at higher energies, a feature located between 3.268 and 3.272 eV was assigned to exciton recombination with a dominant donor bound-exciton (BX) contribution at low temperature.<sup>8</sup> A similar feature is also present in our samples. Its asymmetric line shape with a tail to lower energies suggests also a superposition of FX and BX transitions. However, this assumption is in contradiction with the magnetic-field data, where no change of the line shape is seen, though FX and BX are characterized by distinctly different  $g$  factors ( $g_{\text{FX}} = g_e \pm g_h$ ,  $g_{\text{BX}} = g_e$  or  $g_h$ ). The effective  $g$  factor of the 3.26-eV line is  $g \approx 0.11$ , yielding a Zeeman splitting of about 0.06 meV at 9 T, obviously too small to be directly visible in the optical spectra. The fact that this PL line is the only one that survives at higher temperatures (100 K) represents evidence that it develops indeed into the FX transition. Its nature at low temperature needs, however, further investigation. The 3.15-eV line was attributed<sup>8</sup> to donor-acceptor pair recombination. For the present *c*-GaN films, this assignment is consistent with a high-energy shift of its peak position with increasing excitation intensity. The 3.15-eV line exhibits the largest  $g$  factor ( $g \approx 0.16$ ) from the three dominant transitions. The nature of the 3.08-eV line showing the weakest magnetic-field effect ( $g \approx 0.09$ ) is currently not clear. The shoulder on its low-energy side at about 3.06 eV is probably a LO-phonon replica of the 3.15-eV line. Besides the 90-meV energy separation, this identification is suggested by a degree of polarization close to the 3.15-eV line but distinctly stronger than the background from the 3.08-eV band.

Summarizing, we have elaborated on the surface reconstruction diagram of *c*-GaN. This will allow us to (i) reproduce optimum growth conditions, (ii) avoid formation of wurtzite-related structural transitions, and (iii) correlate optical and electrical properties with the actual growth conditions in further work. At higher growth temperatures, associated with higher mobilities of the Ga adatoms, we could observe for the first time RHEED oscillations of *c*-GaN, nec-

essary to control monolayer growth. PL measurements have demonstrated a reasonably well perfection of the films, promising for future optical application. An estimation of the *g* factor for the dominant recombination channels in *c*-GaN was presented.

The authors acknowledge the support of this work by Deutsche Forschungsgemeinschaft.

- 
- <sup>1</sup>S. Nakamura, T. Mukai, and M. Senoh, *Appl. Phys. Lett.* **64**, 1687 (1994).
  - <sup>2</sup>S. Nakamura, *Jpn. J. Appl. Phys.* **35**, L74 (1996).
  - <sup>3</sup>S. Strite, J. Ruan, Z. Li, A. Salvador, H. Chen, D. J. Smith, W. J. Choyke, and H. Morkoc, *J. Vac. Sci. Technol. B* **9**, 1924 (1991).
  - <sup>4</sup>T. S. Cheng, L. C. Jenkins, S. E. Hooper, C. T. Foxon, J. W. Orton, and D. E. Lacklison, *Appl. Phys. Lett.* **66**, 1509 (1995).
  - <sup>5</sup>T. Lei, K. F. Ludwig, and T. D. Moustakas, *J. Appl. Phys.* **74**, 4430 (1993).
  - <sup>6</sup>H. Siegle, L. Eckey, A. Hoffmann, C. Thomsen, B. K. Meyer, D. Schikora, M. Hankeln, and K. Lischka, *Solid State Commun.* **96**, 943 (1995).
  - <sup>7</sup>O. Brandt, H. Yang, B. Jenichen, Y. Suzuki, L. Däweritz, and K. H. Ploog, *Phys. Rev. B* **52**, R2253 (1995).
  - <sup>8</sup>J. Menninger, U. Jahn, O. Brandt, H. Yang, and K. Ploog, *Phys. Rev. B* **53**, 1881 (1996).
  - <sup>9</sup>J. Y. Tsao, T. M. Brennan, J. F. Klem, and B. E. Hammons, *J. Vac. Sci. Technol. A* **7**, 2136 (1989).
  - <sup>10</sup>Z. Zhu, T. Nomura, M. Miyao, and M. Hagino, *J. Cryst. Growth* **96**, 513 (1989).
  - <sup>11</sup>T. Lei, C. R. Jones, R. Kaspi, and K. R. Evans, in *Gallium Incorporation During Gas-Source Molecular Beam Growth of GaN*, edited by K. Onabe, S. Fujishiro, and H. Morkoc, Proceedings of the Topical Workshop on III-V Nitrides, Nagoya, Japan [IEEE Proc. (to be published)].
  - <sup>12</sup>G. Ramirez-Flores, H. Navarro-Contreras, A. Lastras-Martinez, R. C. Powell, and J. E. Greene, *Phys. Rev. B* **50**, 8433 (1994).
  - <sup>13</sup>H. Okumura, K. Ohta, K. Ando, W. W. Rühle, T. Nagamoto, and S. Yoshida, in *Bandgap Energy of Cubic GaN*, edited by K. Onabe, S. Fujishiro, and H. Morkoc, Proceedings of the Topical Workshop on III-V Nitrides, Nagoya, Japan [IEEE Proc. (to be published)].
  - <sup>14</sup>S. Logothetidis, J. Petalas, M. Cardona, and T. D. Moustakas, *Phys. Rev. B* **50**, 18 017 (1994).
  - <sup>15</sup>A. V. Andrianov, D. E. Lacklison, J. W. Orton, D. J. Dewsnip, S. E. Hooper, and C. T. Foxon, *Semicond. Sci. Technol.* **11**, 366 (1996).